High-density photopolymer-based spatially multiplexed multiwavelength programmable memory

De-Gui Sun and Ray T. Chen

Department of Electrical and computer Engineering
The University of Texas at Austin
Austin, Texas 78712-1084

ABSTRACT

In this paper, a new scheme to implement high-density photopolymer-based spatially multiplexed multiwavelength programmable holographic memory is proposed. Two approaches are considered. The first is to implement programmable massive fanout beams based on an electrooptic grating array and the second is aimed at providing a multi-wavelength high density memory by obtaining a smaller holographic memory spot at the proposed off-focal plane location. In the first approach, the diffraction efficiency of the electrooptically modulated grating is optimized, and 32.5%±2.5% modulation efficiency is achieved under an applied voltage of 100volts. In the second approach, the storage density is improved by 100~110% when compared with that obtained at the focal plane after Fourier transform. All the experimental results agree well with the theoretical predictions. A memory density of 100 pages / mm^2 is feasible using the reported scheme.

KEY WORDS: high-density memory, holography, electrooptic grating array, smaller memory spot, and normalized modulation efficiency.

1. INTRODUCTION

High density programmable holographic memories have long been considered for applications in the area of information processing aimed at a spatially multiplexed multiwavelength interconnect architecture and optical implementation of smaller memory pixels. For spatially multiplexed multiwavelength interconnects, massive fanout devices have shown a myriad of advantages in various applications as a means of offering advanced sensing functions not available in electronic systems. Among many kinds of massive fanout devices that have been investigated, multichannel waveguides[1], and various multi-order grating couplers[2,3], grating couplers deem to be promising to provide one-to-many reconfigurable optical interconnects. Multiplexibility of grating medium plays an important role in device configuration. For volume phase grating materials, where large index modulation and therefore information multiplexibility are reported, Bragg-grating-based massive fanout interconnects can be realized using a single fanout node. For thin phase grating, where index modulation is lower, one-to-many fanout can still be realized using the Roman-Nath diffraction. In the second case, the energy distribution of multiple fanouts is correlated with each other. Minimization of power fluctuations among multiple diffraction orders is a paramount issue to

0-8194-2064-6/96/$6.00

carry out the required fanout involving multiple diffraction orders with a minimum power budget. In this work, a $LiNbO_3$ electrooptic (EO) phase grating array with a massive fanout capability is investigated. From the viewpoint of storage density, the size of memory spots which determines the utimate memory density is a major topic to be embarked upon. The size of Fourier transform memory spot is also determined by spatial spectrum composed of many diffraction orders. The storage capacity of volume holographic memory is usually defined by the signal-to-noise ratio (SNR) or the volume of Fourier transform spectrum[4-6], while the storage density is defined by pixel number per unit area. In this paper, we present an optimized method to improve the storage density by 100~110% and a 100 pages / mm^2 high density memory can be realized with 25 closely space wavelengths (tunable range is 100nm and $\Delta\lambda$=4nm) calculated at 633nm.

2. ANALYSIS FOR MASSIVE FANOUT OF ELECTROOPTIC GRATING

The voltage applied to the interdigitated electrodes associated with an x-cut $LiNbO_3$ crystal induces a periodic index-modulation[7]. The value of this periodic index-modulation Δn_x determines the optical path difference along the x axis, i.e., $\Delta n_x d$, where d is the depth of index modulation (see Fig. 1). If the width of the electrode is a and the spacing between two adjacent electrodes is b, a thin phase grating generated through index modulation with a period $\Lambda = a + b$ is formed. A schematic showing the modulated phase grating aimed at achieving the massive fanout from the waveguide substrate is illustrated in Fig. 1 where the refractive-index of index-matching filler is n_2, the refractive-index of $LiNbO_3$ substrate n_s and θ_1 is the bouncing angle associated with the total internal reflection (TIR).

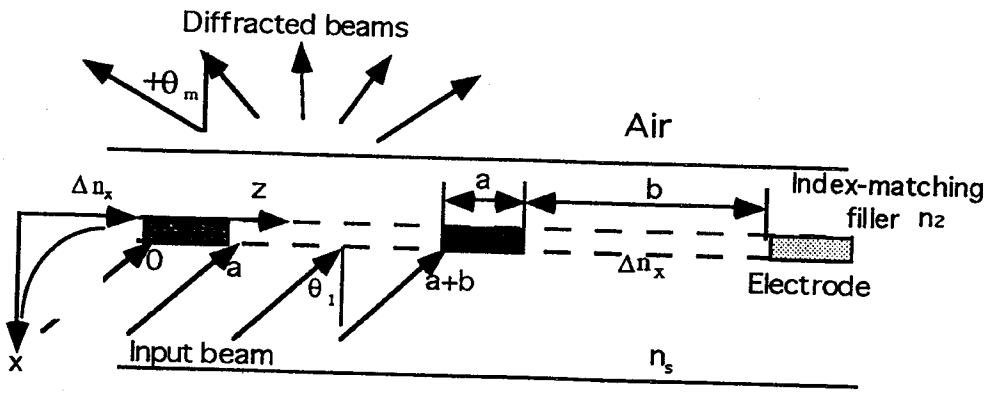

Fig. 1 Diffraction schematic of modulated thin phase grating, a = 2μm and b = 6μm in our experiment

By setting the input intensity as 1, the complex amplitude distribution from a single period resulted from refractive index perturbation can be described by

$$E_1 = \int_0^{a+b} e^{ik\Delta L(z)}dz = \int_0^{a} e^{ik\Delta L(z)}dz + \int_a^{a+b} e^{ik\Delta L(z)}dz \tag{1}$$

where $k = \frac{2\pi}{\lambda}$ is the wave vector of the incident light, λ is the wavelength, and $\Delta L(z)$ is defined by

$$\Delta L(z) = \begin{cases} \dfrac{r(\theta_m)z + \delta(\Delta n)}{k} & (\mathbf{0 < z \le a}) \\ \dfrac{r(\theta_m)z}{k} & (\mathbf{a < z \le a+b}) \end{cases} \tag{2}$$

and

$$r(\theta_m) = [n_s \sin\theta_1 + n_2 \sin\theta_m]k, \text{ and} \tag{3a}$$

$$\delta(\Delta n) = \frac{\Delta n_x d}{\cos\theta_1}k \tag{3b}$$

In Eqs. (3a) and (3b), θ_m is the mth order diffraction angle. Based on Eqs. (2), (3a) and (3b), Eq. (1) thus becomes

$$E_1(\theta_m) = \int_0^{a} e^{i(rz+\delta)}dz + \int_a^{a+b} e^{irz}dz = \frac{(e^{iar}-1)e^{i\delta}}{ir} + \frac{(e^{ibr}-1)e^{iar}}{ir} \tag{4}$$

Based on Eq. (4), the intensity distribution of a normalized diffraction from the single-period grating can be represented as:[8]

$$I_1 = E_1 * E_1^* \approx \left[\frac{2\sin(\frac{\delta(\Delta n)}{2})\sin(\frac{a \bullet r(\theta_m)}{2})}{\frac{r(\theta_m)}{2}} \right]^2 \tag{5}$$

Considering the normalized diffraction of the single-period grating and the normalized multislit diffraction, we derive the final normalized intensity distribution as

$$I(\theta_m, \Delta n_x) = \sum_m I_1 \bullet I_2 \approx \sum_m \left[\frac{2\sin(\frac{\delta(\Delta n)}{2})\sin(\frac{a \bullet r(\theta_m)}{2})}{\frac{r(\theta_m)}{2}} \right]^2 \bullet \left[\frac{\sin(N\frac{\Lambda r(\theta_m)}{\lambda})}{\sin(\frac{\Lambda r(\theta_m)}{\lambda})} \right]^2 \tag{6}$$

where N is the total number of grating grooves. In this work, a $LiNbO_3$ crystal with an index $n_s = 2.24$ is taken as the guided wave substrate together with $\lambda = 0.633\mu m$, $a = 2\mu m$, $b = 6\mu m$, $N = 125$, $n_2 = 2.086$, $r_{13} = 9.6\times10^{-12}$, $V = 100v$, and $\theta_1 = 45°$. We obtain $\Delta n_x d \approx 2.3\times10^{-3}\mu m$. The fabricated $LiNbO_3$ EO grating array is shown in Fig. 2 where the detailed microstructure associated with each grating is also provided. The grating was made out of an ITO film coated on an x-cut $LiNbO_3$ substrate.

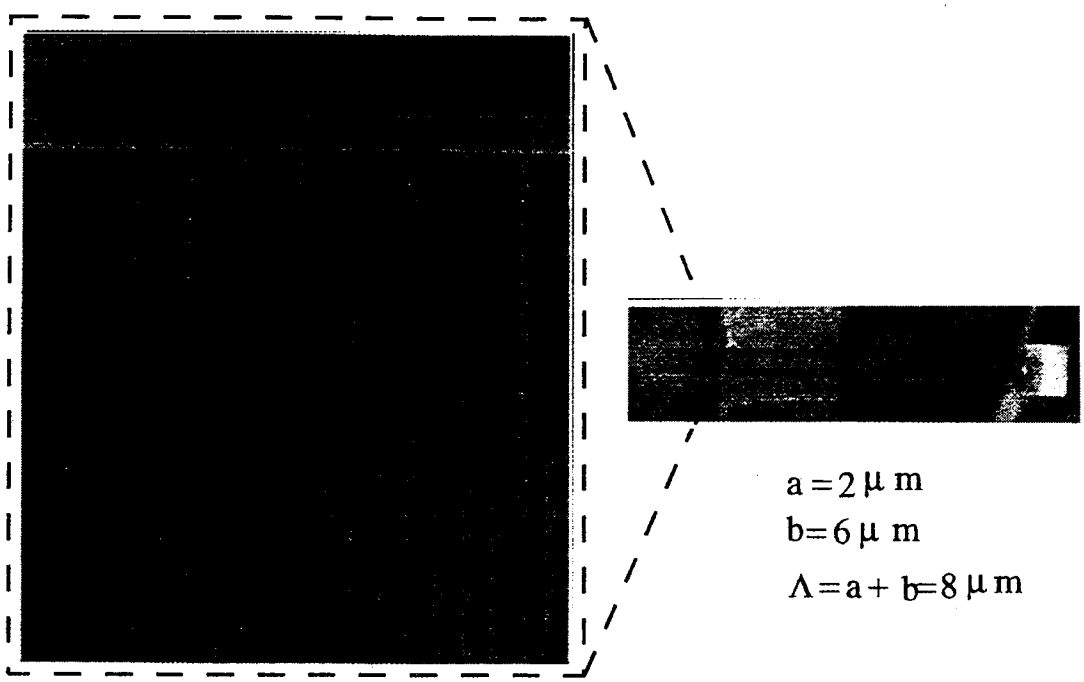

Fig. 2 Picture of the fabricated $LiNbO_3$ EO grating array

Furthermore, the θ_m-dependent distribution curve for the final normalized intensity is shown in Fig. 3(a). Note that there are many diffraction orders for one fixed wavelength λ. The observed result and the measured values of various diffraction orders corresponding to the above-mentioned experimental setting are further illustrated in Figs. 3(b) and 3(c), respectively. Because this massive fanout EO grating is used to provide a multi-wavelength programmable holographic memory, the relationship between the diffraction angle θ_m and wavelength λ is worthy of specially discussion under a fixed diffraction order. According to Eq. (6), the condition to produce the mth order diffraction peak can be described by:

$$a \bullet r(\theta_m) = (2m-1)\pi \tag{7}$$

Combining Eqs. (3a) and (7), we have

$$\theta_m = \sin^{-1}[\frac{1}{n_2}(\frac{2m-1}{2a}\lambda - n_s \sin\theta_1)] \qquad (8)$$

The curves defined by Eq. (8) are shown in Fig. 4. Note that θ_m does not dramatically depend on the wavelength λ, which is more suitable for its application in multiwavelength holographic memory.

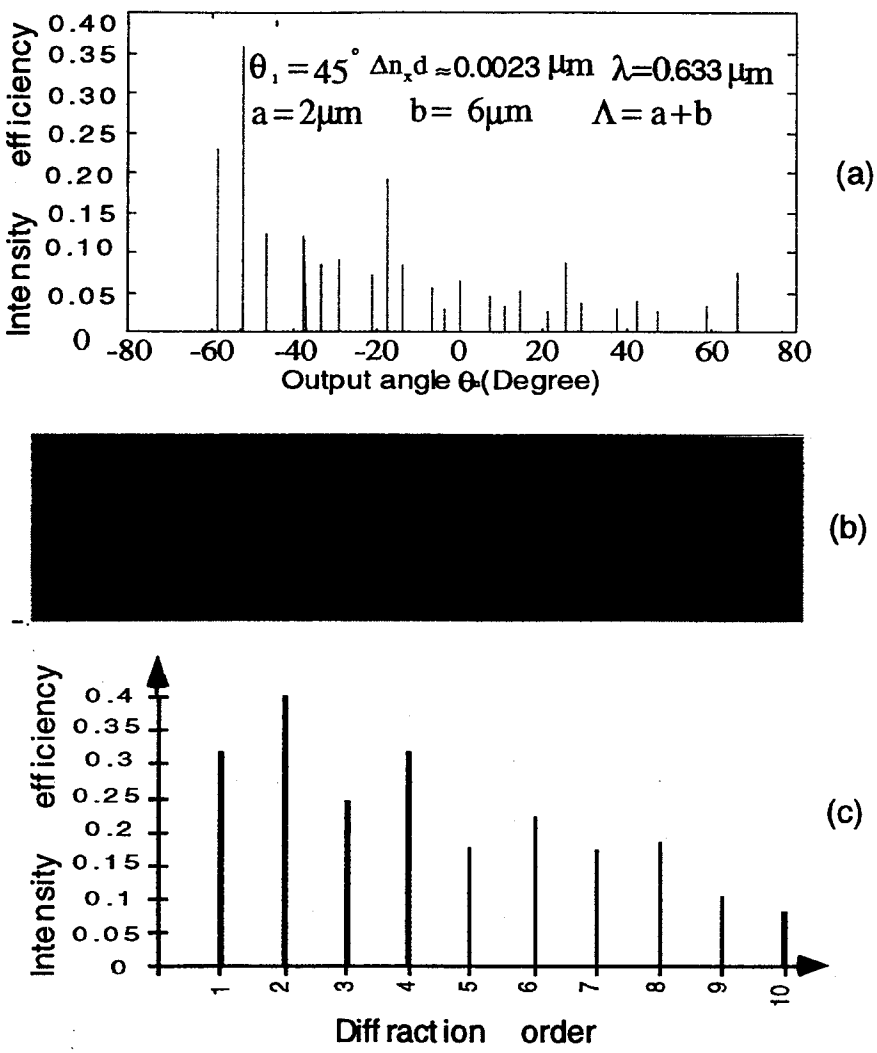

Fig. 3 Angular distribution of multiple diffraction orders coupled by EO modulated grating: (a) theoretical result, θ_m represents the output angle associated with the mth diffraction order; (b) picture of the far field pattern of multiple diffraction orders; (c) measured result

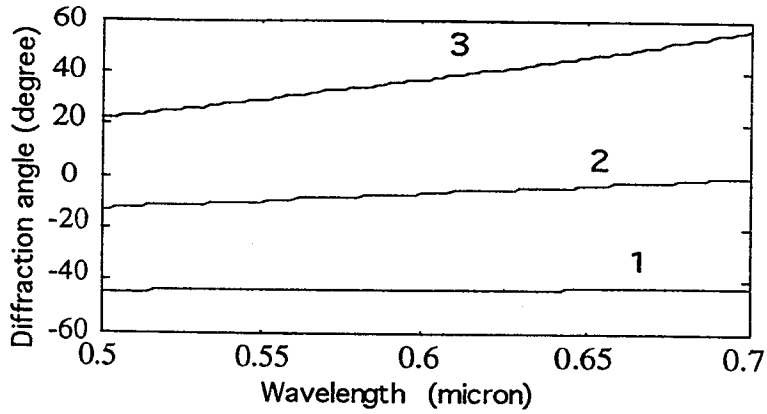

Fig. 4 Relationship between θ_m and λ of three different diffraction orders: 1. the 1th order; 2. the 5th order; and 3. the 10th order

In this experiment, the measured modulation efficiency is defined by

$$\eta = \frac{P_m}{P_b} \tag{9}$$

where P_m is the total power of all the diffracted beams after the applied voltage is activated, P_b is the total power of the substrate guided wave before interacts with the EO grating. The experimental setup for AC measurement is shown in Fig. 5(a), where an AC current, a highly sensitive detector and an oscilloscope are used. A pair of test-probe positioners are used to effectively apply the modulation voltage onto the EO gratings. The experimental result of the EO grating diffraction is observed in Fig. 5(b) which represents 32.5%±2.5% modulation depth at 100 volts. This result is

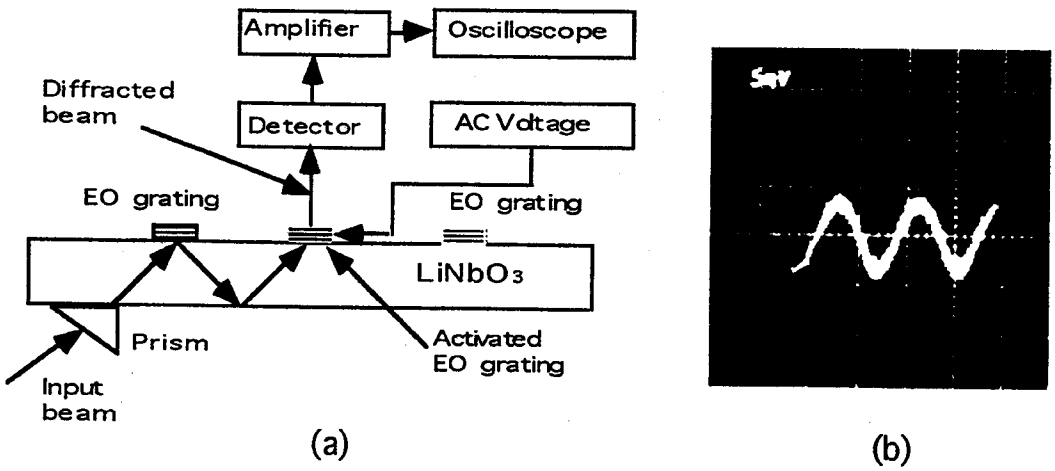

Fig. 5 Experimental setup for the evaluation of the EO thin phase grating array: (a) the setup; and (b) modulation transfer curve represents 32.5%±2.5% (f=60Hz)

well-matched with the theoretical prediction. Reconfiguration of the fanout beams are experimently realized by activating each EO grating independently.

3. FEASIBILITY STUDIES OF HIGH DENSITY HOLOGRAPHIC MEMORY

The evaluation of linear array is very similar to that of a single pixel device. The proposed configuration for holographic recording and reading employing the one-dimensional $LiNbO_3$ EO grating arrays are further depicted in Figs. 6(a) and 6(b), respectively, where the reference beam is introduced through total internal reflections (TIRs) with a pre-determined bouncing angle. The real device under investigation is shown in Fig. 6(c) where a linear EO grating array with the associated elements are clearly shown. The EO grating that activates the reference beam is turned on through the two microprobes.

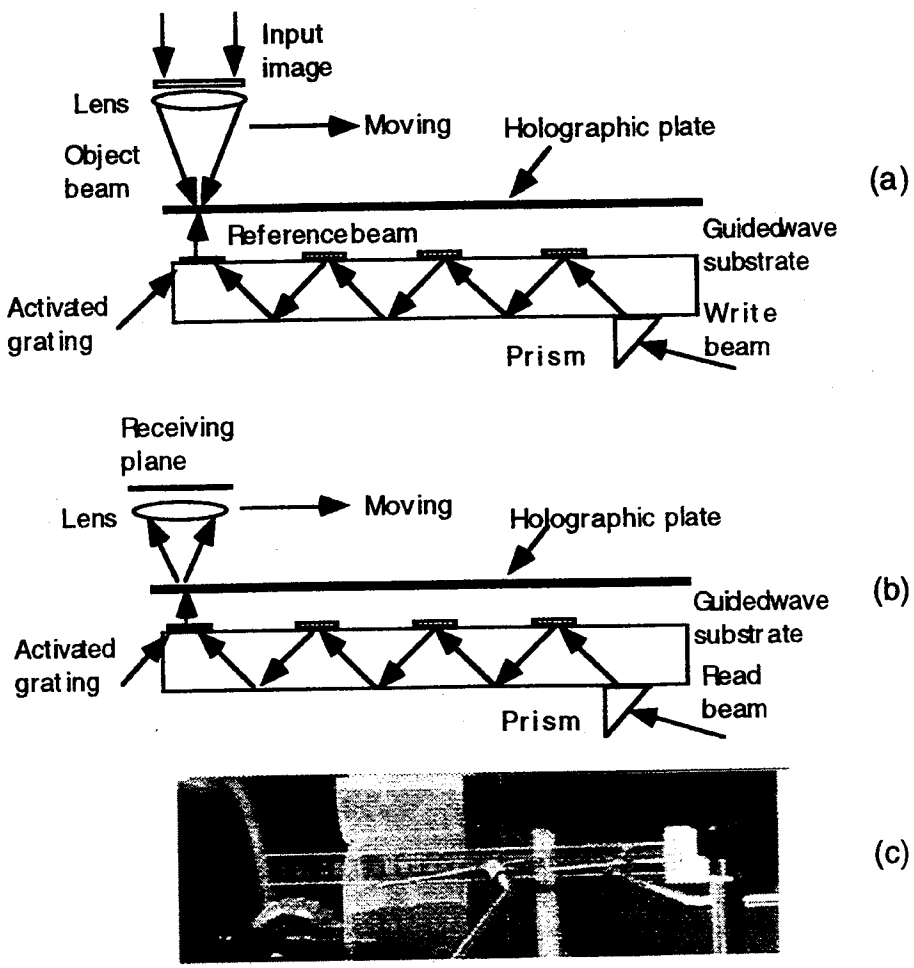

Fig. 6 Proposed configuration for hologram recording: (a) schematic for hologram recording; (b) schematic for hologram reading; and (c) picture of a real device

In our experiments, the size of input image of a bird pattern as shown in Fig. 7(a) is $7.68 \times 7.68 mm^2$ carrying one page information of 256×256 bits. We obtain holographic memory spots with a diameter of 0.5mm for the two different wavelengths ($\lambda = 0.633\mu m$ and $\lambda = 0.514\mu m$) and the reconstructed image of $\lambda = 0.633\mu m$ is shown in Fig. 7(b) and the reconstructed image of $\lambda = 0.514\mu m$ is shown in Fig. 7(c), which agree well with the theoretical prediction.

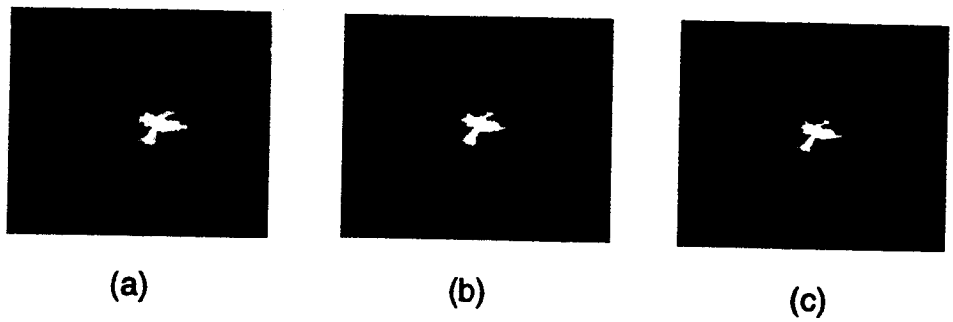

Fig. 7 Experiments: (a) input image; (b) reconstructed holographic image of $\lambda = 0.633\mu m$; and (c) reconstructed holographic image of $\lambda = 0.514\mu m$

4. ANALYSIS FOR STORAGE DENSITY OF HOLOGRAPHIC MEMORY

In a holographic recording system, when an image composed of a myriad of pixels is illuminated by a collimated beam, it functions a grating. A schematic diagram of the imaging system for the object beam of holographic memory is shown in Fig. 8, where FL is a Fourier transform lens, P_1 plane is input image plane, P_2 is the focal plane of lens FL, and P_4 is the plane where the 1st diffraction order converges. P_3 is the intersection plane of the 0th diffraction order and the 1st diffraction order.

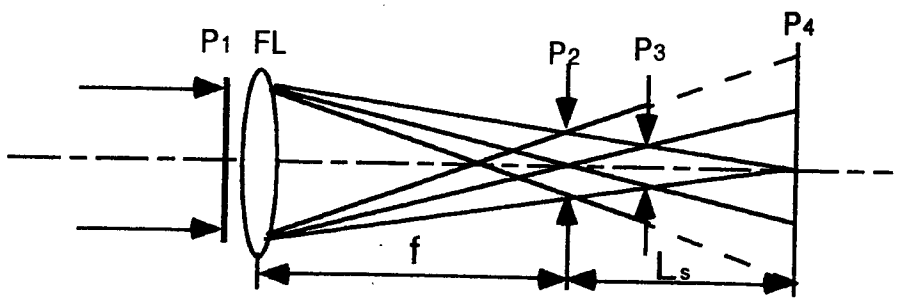

Fig. 8 Analysis of imaging system for the holographic memory

The sizes of memory spots at the different detecting planes are obviously different and mainly determined by the peaks associated with the 0th diffraction order and the 1st diffraction order. When the center to center spacing between two adjacent pixels is p, we have[8]

$$p\sin\theta_1 = \lambda \tag{10}$$

where θ_1 and λ are the edge diffraction angle of the 0th order and the operating wavelength, respectively. Assuming the size of input image is $S_1 \times S_1$, the total number of pixels of a linear array is $N = S_1 / p$ and the aperture of the Fourier transform lens $D_1 = \sqrt{2}S_1$. At the Fourier transform plane P_2, the size of the memory spot D_2 and the one-dimensional (1-D) pixel storage-density C_2 can be represented as:

$$D_2 \approx \frac{R\lambda f}{p} \tag{11a}$$

and

$$C_2 \approx \frac{1}{R\lambda(f/\#)} \tag{11b}$$

where R is the Rayleigh criterion ranging from 1.2 to 1.5 which is hologram enlargement factor of memory spots at plane P_2. To get a smaller holographic memory spot and therefore small pixel size, we analyze the whole imaging process of the memory system. The outside ring produced by the first order diffraction should be blocked by using an aperture at plane P_3, while the central part actually includes most of information for the hologram. With a given f/#, the size of the central part (i.e., the smallest imaging spot) D_3 and the one-dimensional pixel storage-density C_3 can be represented as:

$$D_3 = \frac{\lambda(f/\#)}{p-\lambda(f/\#)}D_1 \tag{12a}$$

and

$$C_3 = \frac{p-\lambda(f/\#)}{\lambda(f/\#)D_1}N \tag{12b}$$

At first, with Eqs. (11b) and (12b), we take R=1.2, $\lambda = 0.633\mu m$ and $S_1 \times S_1 = 7.68 \times 7.68 mm^2$, and obtain the distribution curves of pixel storage-densities at the focal plane P_2 and the off-focal plane P_3 as functions of p with respect to several different f/# values as shown in Fig. 9(a) and Fig. 9(b), respectively. The curves shown in Fig. 9(a) are derived using Rayleigh criterion R=1.2. Note that, for a fixed f/#, the pixel storage-density calculated at the off-focal plane is higher than the counterpart calculated at the focal plane in one-dimensional direction.

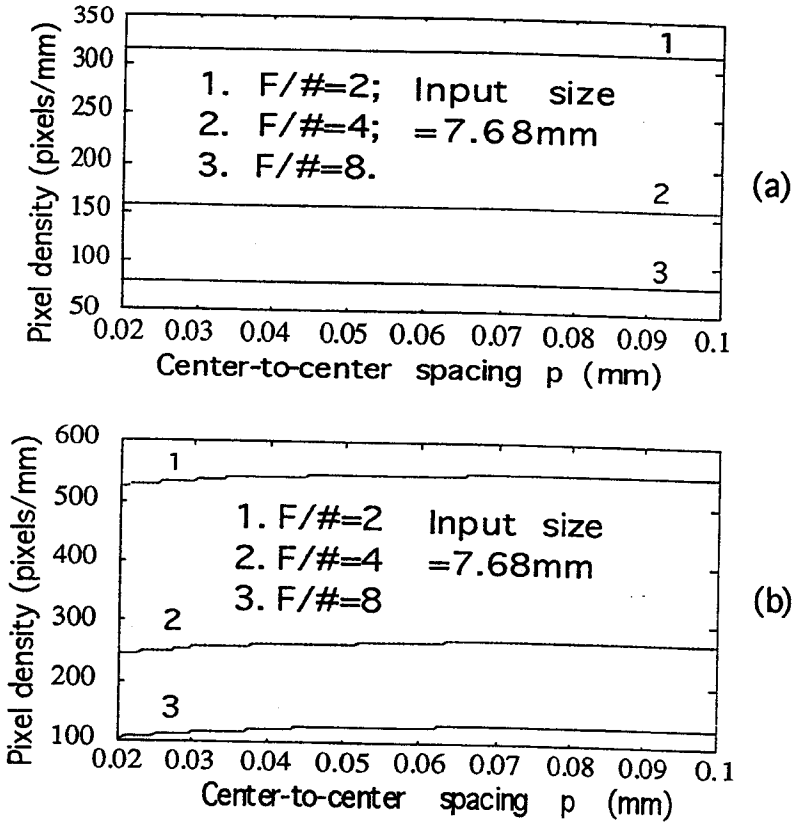

Fig. 9 Distribution curves of 1-D storage densities as functions of center-to-center spacing p: (a) at the Fourier transform plane P_2; (b) at far field plane P_3

For the wavelength multiplexing, the frequency agile laser with a λ tunable range of 100nm and $\Delta\lambda$=4nm obtains 25x multiplexing per recording stack, which prefers to calculate the uniformity of spot sizes for the whole wavelength range we used in this memory system. With Eqs. (11a) and (12a), we fix f/#=2.7 and $p = 30\mu m$, and obtain the λ-dependent relationships of memory spots at the two different planes P_2 and P_3 as shown in Fig. 10, curves 1 and 2, respectively. Fig. 10 covers all the possible wavelengths used in this work. Note that the memory spots at plane P_3 are more uniform for different wavelengths, which is another advantage of taking holographic memory at plane P_3. In addition, the λ-dependent relationship curves in Fig. 10 can be used to evaluate the new approach to achieve a higher storage density. For example, the improvement of storage density is defined by

$$\eta_d = \left(\frac{D_2^2}{D_3^2} - 1\right) \times 100\% \tag{13}$$

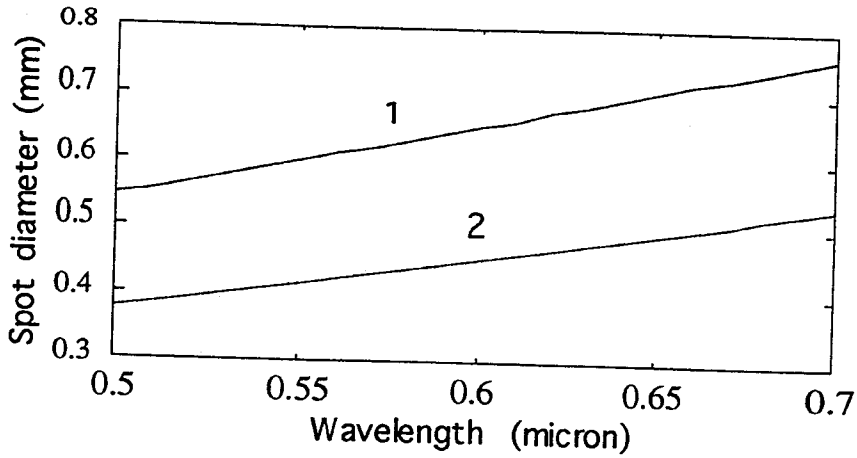

Fig. 10 λ-dependent relationships of memory spots at the two different planes: curve 1 is at plane P_2 and curve 2 at P_3

With Fig. 10, we know the size of memory spot D_2 at P_2 plane is varying from 0.55mm to 0.76mm in accordance with curve 1, and the size of memory spots D_3 at P_3 plane is from 0.38mm to 0.54mm in accordance with curve 2. Furthermore, we obtain that the improvement of the storage density is about 100% using Eq. (13). Finally, according to curve 2 in Fig. 10, we also obtain the storage density of 100pages / mm^2, i.e., .4pages / mm^2 for one wavelength.

5. CONCLUSIONS

A new architecture to implement high-density photopolymer-based spatially multiplexed multiwavelength programmable memory is proposed to combine the spatial multiplexibilty of massive fanout technique and smaller pixel size by recording a hologram method at an off-focal plane located at P_2 (Fig. 8). Storage density is improved by 100~110% and a memory density of 100 pages / mm^2 is feasible using the reported scheme. As a massive fanout device, the electrooptic phase grating is studied in detail and 32.5% $\pm$2.5% diffraction efficiency under an applied voltage of 100V is obtained at λ=633nm. The result is well-matched with theoretical calculation. Finally, a programmable holographic memory is recorded and reconstructed by employing multiple diffraction orders of the EO grating as the reference beam.

6. ACKNOWLEDGMENTS

The authors thank Dr. T.C. Lee, Dr. Richard Lee, Mr. Huajun Tang and Mr. Chunhe Zhao for their help in this work.

7. REFERENCES

1. R. T. Chen, H. Lu, D. Robinson, M. Wang, G. Savant, and T. Jannson, "Guided-wave planar optical interconnects using highly multiplexed polymer waveguide holograms," IEEE J. LW Tech. 10(7), 888-897 (1992).

2. T. Kubota and M. Takeda, "Array illuminator using grating couplers," Opt. Lett. 14(12), 651-652 (1989).

3. R. T. Chen, D. Robinson, H. Lu, M. R. Wang, T. Jannson, and R. Baumbick, "Reconfigurable optical interconnection network for multimode optical fiber sensor arrays," Opt. Eng. 31(5), 1098-1106 (1992).

4. X. Yi, P. Yeh, and C. Gu, "Statistical analysis of crosstalk noise and storage capacity in volume holographic memory," Opt. Lett. 19(9), 1580-1582 (1994).

5. J. Hang and D. Psaltis, "Storage capacity of holographic associative memories," Opt. Lett. 11(2), 812-814 (1986).

6. D. Brady and D. Psaltis, "Storage capacity of 3-D holographic data storage," Opt. Quant. Electron. 25, 597-610 (1993).

7. E. N. Glytsis and T. K. Gaylord, "Anisotropic guidedwave diffraction by interdigitated electrode-induced phase gratings," Appl. Opt. 27(24), 5031-5050 (1988).

8. M. C. Hutley, Diffraction Gratings, Academic Press, New York, 1982.